Sustainable Energy & Fuels

ROYAL SOCIETY OF CHEMISTRY

PAPER

View Article Online
View Journal | View Issue

Cite this: *Sustainable Energy Fuels*, 2023, 7, 3883

Understanding the role of interfacial layers in the photostability of PM6:Y7-based organic solar cells under different degradation conditions†

Magaly Ramírez-Como, [a] Enas Moustafa, [a] Mohamed Samir, [a] Alfonsina Abat Amelenan Torimtubun, [a] José G. Sánchez, [b] Josep Pallarès *[a] and Lluis F. Marsal *[a]

Organic solar cells (OSCs) have reached an efficiency near 20%; however, their low long-term stability is the main limitation to their industrialization. In this work, we investigated the degradation of bulk heterojunction non-fullerene solar cells (NFA-OSCs) based on PM6:Y7 with an efficiency of 17.5%. The degradation analysis was carried out following the established ISOS-D-1 protocol under different degradation conditions: N_2 atmosphere (H_2O < 0.1 ppm and O_2 < 0.1 ppm) and encapsulated devices and non-encapsulated devices exposed to ambient conditions (60 ± 5% relative humidity). The evolution of the current density–voltage (*J*–*V*) and impedance spectroscopy (IS) measurements were used to analyse the degradation process during 1000 h and its relationship with physical mechanisms. The degradation of encapsulated and non-encapsulated devices is mainly caused by the drop in the open circuit voltage (V_{OC}). For devices exposed to the N_2 atmosphere, the fill factor (FF) was the most affected parameter. The dependence of short circuit current density (J_{SC}) *versus* light intensity study reveals that the efficiency of non-encapsulated devices decreases faster due to a higher bimolecular recombination degree. The devices under a N_2 atmosphere and those encapsulated showed T_{80} lifetimes of 1000 h and 336 h, respectively, whereas the non-encapsulated devices have a short T_{80} lifetime of less than 24 h. The analysis of the efficiency decay was used to identify the different degradation mechanisms (by diffused environmental water or oxygen or by intrinsic polymer chemical reactions) under different conditions. The degradation origin of the active layer and interlayers was investigated through impedance spectroscopy measurements.

Received 28th May 2023
Accepted 27th June 2023

DOI: 10.1039/d3se00703k

rsc.li/sustainable-energy

Introduction

In the last few years, non-fullerene acceptor (NFA) materials have been investigated intensively to replace the fullerene acceptor material in organic solar cell (OSC) photoactive layers. As a result of these studies, the performance of OSCs has improved significantly, achieving efficiencies of around 18% in single-junction devices.[1–3] To produce efficient OSCs, it is required to have acceptor and donor materials with matching absorption bands in the Vis-NIR range, high charge-carrier mobility, and a small energy offset to minimize voltage losses. Mainly, the development of fused-ring Y7 and Y6 NFA molecules has improved power conversion efficiencies (PCEs) by pairing selected polymer donors, such as PM6.[4–6] The design of the fused-ring core unit of these low-bandgap NFA molecules minimizes the trade-off behaviour between voltage loss and charge generation, thus increasing PCE.[7,8] Moreover, these materials can tune their energy levels and show strong absorption in the near-infrared region with donor polymers.[9,10] These properties lead to high charge carrier mobility and barrier-less free charge generation in cells. Another method to improve the efficiency of OSCs is the ternary strategy with one donor and two acceptors or two donors and one acceptor.[11–13]

However, high efficiency is not the only requirement to scale up OSCs in the market. The stability of cells is still a factor that limits their operating lifetime and the key criterion to make the large-scale fabrication of OSCs commercially more feasible. For this reason, an important aim to be accomplished is looking for selective materials and developing good engineering strategies that improve the stability of the devices for a long time. Different strategies have been used to improve the OSC stability and to minimize intrinsic degradation. For instance, developing new buffer layer materials that are more stable, alternating device structures, modifying the chemical structure of active layer materials, eliminating the photo-dimerization of fullerenes, increasing the material crystallinity of nonfullerene materials, and varying contact electrodes.[14–16] Additionally, to

[a]*Department of Electric, Electronic and Automatic Engineering, Universitat Rovira i Virgili, 43007 Tarragona, Spain. E-mail: josep.pallares@urv.cat; lluis.marsal@urv.cat*
[b]*Institute of Chemical Research of Catalonia, The Barcelona Institute of Science and Technology (ICIQ-BIST), 43007 Tarragona, Spain*

† Electronic supplementary information (ESI) available. See DOI: https://doi.org/10.1039/d3se00703k

reduce extrinsic degradation, an appropriate encapsulation layer has been widely used to prevent the interaction of moisture and oxygen from the atmosphere and minimize the degradation of materials inside OSCs.

In this context, several characterization techniques can be used to analyse the stability of the devices, *e.g.* the current density–voltage (*J*–*V*) characteristic curve to analyse the evolution of photovoltaic parameters;[17,18] external quantum efficiency (EQE) to identify the species involved in degradation by processes such as chromophore bleaching; light intensity dependent short circuit current density (J_{SC})/open circuit voltage (V_{OC}) to study the recombination and trapping upon aging; absorption UV-Vis spectroscopy to reveal chromophore bleaching or changes in morphology such as directional rearrangement; space charge limited current (SCLC) to observe the evolution of carrier mobility; impedance spectroscopy (IS) to observe the evolution upon aging of resistive and capacitive behaviour that reveals the change in transport and recombination regimes.[19–24]

In this research study, we investigate the degradation of the conventional OSCs that were optimized in our previous work using PM6:Y7.[6] We analysed the changes in the *J*–*V* characteristic curve and performed IS measurements to understand the behaviour of their performance over time. The standard procedure of the ISOS D-1 protocol was used for an accurate lifetime determination. The degradation study was made in the dark for up to 1000 h. Three conditions were analysed: devices under an inert N_2 atmosphere and encapsulated and non-encapsulated devices under ambient conditions. The fabricated non-fullerene acceptor OSCs (NFA-OSCs) have the structure of ITO/PEDOT:PSS/PM6:Y7/PDINO/Ag. The study is performed by fitting the evolution of the power conversion efficiency parameter by the decaying of two exponentials with characteristic decay times, which are associated with the possible predominant degradation mechanisms. Impedance spectroscopy characterization was performed under AM 1.5G light conditions, at open circuit voltage, to study the transport processes taking place in the device. An equivalent circuit, consisting of three RC elements in series, was associated with each layer (ETL, active layer, and HTL) of the NFA-OSCs.

Results and discussion

Analysis using current density–voltage (*J*–*V*) measurements and external quantum efficiency (EQE)

In this work, we analysed bulk heterojunction NFA-OSCs under three different conditions: devices under a N_2 atmosphere and encapsulated devices and non-encapsulated devices that were exposed to ambient environments following the ISOS-D-1 protocol.[25] The fabricated cells were only exposed to light during the characterization and returned to the dark shelf. The conventional configuration of NFA-OSCs analysed was ITO/PEDOT:PSS/PM6:Y7/PDINO/Ag. Fig. 1(a) shows the schematic representation of the fabricated devices. Fig. 1(b)–(d) show the behaviour of current density–voltage (*J*–*V*) characteristics through the all-time analysis conducted at one sun under

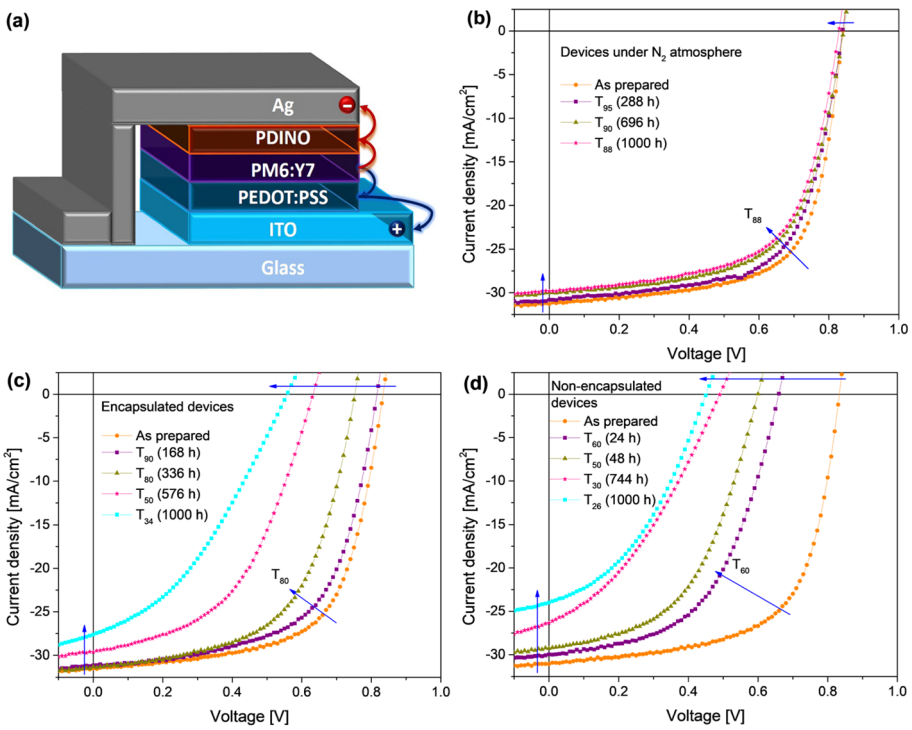

Fig. 1 (a) Schematic representation of the fabricated devices. The current density–voltage (*J*–*V*) characteristics curves under illumination conditions of PM6:Y7 based NFA-OSCs under three different degradation conditions: (b) N_2 atmosphere, (c) encapsulated devices and (d) non-encapsulated devices both exposed to ambient environments over shelf storage time. T_{80} is the time the devices took to decay 20% from their initial PCE.

simulated AM 1.5G illumination. The as-fabricated devices namely "fresh devices" were characterized immediately after the fabrication process. The performance parameters of encapsulated and non-encapsulated devices degraded (1000 h) under ambient conditions considerably decrease in comparison to those of devices stored under a N_2 atmosphere. Fig. 1(b) shows that the V_{OC} of NFA-OSCs stored under a N_2 atmosphere remained at about 830 mV during the whole analysis (1000 h). Meanwhile, J_{SC} decreased slightly from 31.30 mA cm^{-2} to 29.78 mA cm^{-2}. Fig. 1(c) shows that the V_{OC} of the encapsulated device slightly reduced after 168 h, while its J_{SC} decreased after 336 h. However, after 1000 h, V_{OC} decreased from 828 mV to 556 mV and J_{SC} decreased from 31.25 mA cm^{-2} to 27.57 mA cm^{-2}. Importantly, S-shaped J–V curves were not noticed in any measurement of encapsulated NFA-OSCs and NFA-OSCs stored under a N_2 atmosphere. On the other hand, as expected the V_{OC} and J_{SC} of non-encapsulated NFA-OSCs exposed to ambient conditions decreased faster than those of encapsulated NFA-OSCs (see Fig. 1(d)). The V_{OC} decreased from 830 mV to 440 mV and J_{SC} from 30.59 mA cm^{-2} to 25.06 mA cm^{-2} after 1000 h. Additionally, an S-shape began to emerge in the last J–V measurement at 1000 h of exposure under ambient conditions for voltage above V_{OC} (see Fig. S1(c)†). Several authors have reported that the S-shape in the J–V curve could be caused by charge accumulation at the interfaces or unbalanced charge transportation.[26,27]

To obtain more information about the degradation trend behaviour of NFA-OSCs exposed to three different conditions, Fig. 2(a)–(d) show the normalized device performance parameters (PCE, V_{OC}, J_{SC}, and fill factor (FF)) as a function of the exposure time. Corresponding to the ISOS-D-1 protocol, the operating shelf lifetime of each studied NFA-OSCs is displayed in Fig. 1(b)–(d) and shown in Table S1.† The maximum initial PCE measurement (E_0) for each device was 17.53%, 16.97%, and 16.46% for devices in a N_2 atmosphere and encapsulated and non-encapsulated devices, respectively. The T_{80} is the time at which the PCE decays 20% with respect to E_0. Fig. 2(a) shows the PCE decay behaviour of all cells. It should be noted that for non-encapsulated devices a rapid decay of PCE is observed in the first 48 h. Meanwhile, a slower PCE decay is observed in encapsulated devices. This behaviour is a degradation loss mechanism known as "burn-in loss" due to the photochemical reactions within the active layer affecting charge transport properties.[28,29] The non-encapsulated devices lose 20% of their initial PCE before 24 h (T_{80}), faster than encapsulated devices which took 336 h. The poor stability of non-encapsulated NFA-OSCs is related to water and oxygen under ambient conditions degrading the electrode interfaces and reducing the electrical properties of the active layer of OSCs.[30,31] After 1000 h, the PCE of devices under a N_2 atmosphere remained at 88% of its initial value.

As shown in Fig. 2(a), the degradation of all the devices follows an exponential law decay. The fast initial decay followed by a slow decay is modeled by the superposition of two exponential functions with different time constants, as reported previously in the literature.[24,32,33] In Fig. 2(a), the lines show the fitted degradation behaviour over time using eqn (1).

$$\frac{\mathrm{PCE}(t)}{\mathrm{PCE}(0)} = A_1\, \mathrm{e}^{-\frac{t}{T_1}} + A_2\, \mathrm{e}^{-\frac{t}{T_2}} \quad (1)$$

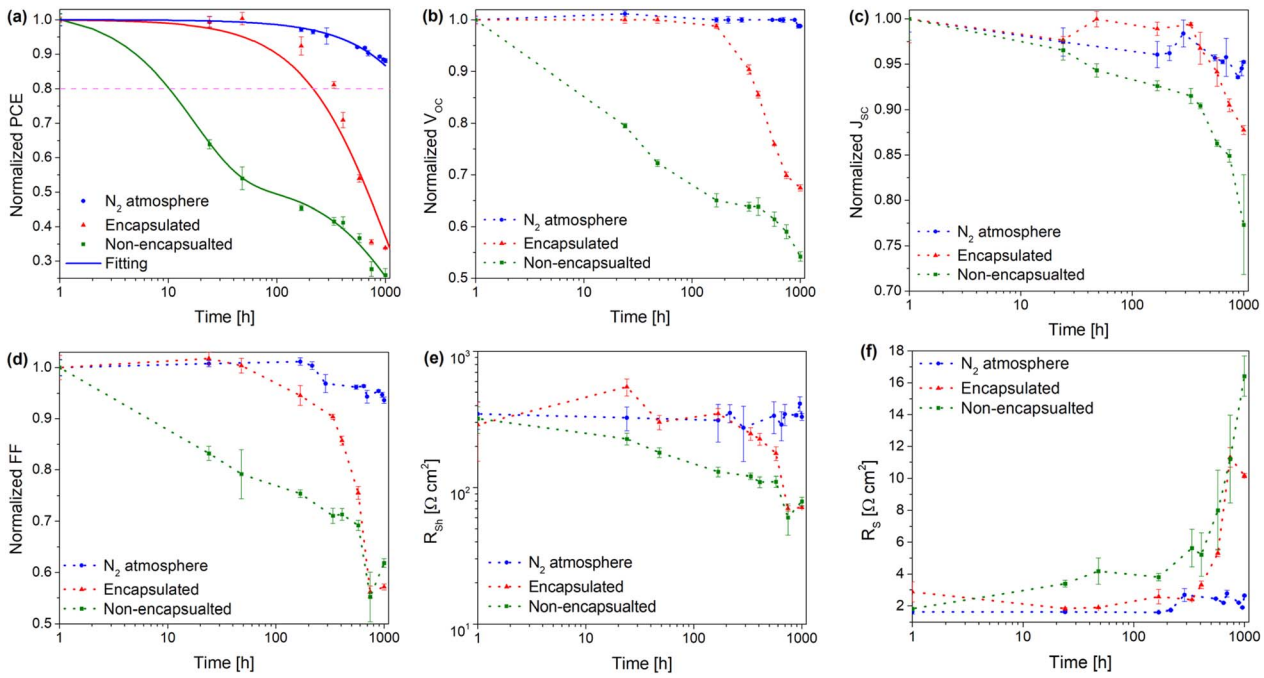

Fig. 2 Normalized performance parameters (a) PCE, (b) V_{OC}, (c) J_{SC}, and (d) FF of the NFA-OSCs under three different conditions: N_2 atmosphere and encapsulated and non-encapsulated devices. In addition, (a) shows the fitting of the normalized PCE over the storage time using eqn (1) and the solid lines show the fitting curve. (e) Shunt and (f) series resistances of the NFA-OSCs under the aforementioned conditions.

where PCE(0) is the relative initial PCE. The degradation power factors of the individual exponential functions (A_1 and A_2) and the time constants (T_1 and T_2) are obtained *via* a least-squares fit. Table 1 summarizes the extracted parameters from the modeled PCE for the NFA-OSCs under three different conditions using eqn (1). The degradation mechanisms represented by the first (T_1) and second (T_2) time constants are related to the diffusion of water and oxygen that diffuse within the device, respectively as was observed similarly in ref. 24 and 32–34. In this sense, if T_1 is a smaller value than T_2 this indicates that water diffusion induces higher degradation over time. For the NFA-OSCs exposed to the N_2 atmosphere, high degradation time constants (T_1 and T_2) were obtained, which suggests that the main degradation mechanism in these devices does not occur due to the water and oxygen since there are lower water and oxygen contents in the N_2 atmosphere (<0.1 ppm). Therefore, the degradation can be attributed to a chemical reaction between the metallic and organic materials.[35] Besides, the acidic nature of PEDOT:PSS favours the corrosion of the ITO electrode, which is detrimental to some donor materials.[36–38]

The time constant T_1 for non-encapsulated NFA-OSCs (17 h) shows the lowest value of the three conditions of degradation, suggesting that these cells suffer more from the presence of water. It is well known that PEDOT:PSS can accelerate the oxidation process due to its hygroscopic nature.[30] In the same way, for encapsulated NFA-OSCs, we can suggest that the degradation mechanism is mainly due to the increased chemical reaction of the materials with water than with oxygen due to T_1 (728 h) being lower than T_2 (1400 h). Some authors have reported that encapsulation by using barrier materials with a water vapour transmission ratio (WVTR) of 10^{-3} g m^{-2} day^{-1} is sufficient to achieve lifetimes of several thousand hours in operation.[17,39] We encapsulated our cells using an NOA adhesive inside the glass–glass structure. The WVTR, reported by the manufacturer of the NOA adhesive is 22.94 g m^{-2} day^{-1}. Kovrov *et al.*[40] reported a WVTR of glass–glass structures using epoxy glues and commercial acrylic with values between 0.2 and 1.5 g m^{-2} day^{-1}. Therefore, it seems that after enough time (336 h) in encapsulated NFA-OSCs, the WVTR of the adhesive is not enough to avoid the cell degradation.

The behaviour of shunt (R_{Sh}) and series (R_S) resistances over time was also analysed (Fig. 2(e) and (f)). The R_{Sh} of non-encapsulated NFA-OSCs degraded rapidly from the beginning. However, in encapsulated NFA-OSCs, R_{Sh} was stable for the first 168 h, after which it decreased rapidly. As shown in Fig. 2(b), the V_{OC} for encapsulated and non-encapsulated NFA-OSCs was the parameter that shows a similar trend to the PCE decay (Fig. 2(a)). Therefore, the variation of PCE with time for both degradation conditions was mainly due to the variation of V_{OC}. Additionally, both V_{OC} and R_{Sh} of encapsulated devices decreased after 168 h, while for non-encapsulated devices these decreased after 24 h (see Fig. 2(b) and (e)). It has been previously reported that the V_{OC} can be reduced if R_{Sh} reduces.[41,42] The reduction of R_{Sh} can be associated with the recombination of charge carriers near the donor/acceptor interface of the active layer.[43] Furthermore, the V_{OC} can also decrease due to charge recombination at the HTL/donor interface if bulk heterojunctions present barriers at this interface.[44] On the other hand, for NFA-OSCs stored under a N_2 atmosphere, R_{Sh} and V_{OC} showed a minimal variation in the initial value at the end of the analysis time.

Fig. S2(a)–(c)† show the *J*–*V* characteristic in the dark through the all-time analysis. In Fig. S2† it can be observed how the current density between 0.9 and 1 V decreases with time, which reveals the increment of the R_S. This is confirmed from the plot of R_S *vs.* time, in Fig. 2(f). The R_S of non-encapsulated NFA-OSCs increased from the beginning, and after 336 h R_S values increased abruptly. On the other hand, for encapsulated NFA-OSCs the R_S remained with slight variation and after 336 h, increased gradually. For NFA-OSCs exposed to an N_2 atmosphere, the R_S remained at around 2 Ω cm^2 throughout the analysis. The decrease in the J_{SC}, observed in Fig. 2(c), for encapsulated and non-encapsulated NFA-OSCs can be attributed to an increment in the R_S. Generally, the increase in R_S can be related to different factors such as (i) the formation of an isolation layer between the metallic contact and the active layer, which reduces the collection of charge carriers;[45,46] (ii) the reduction of the density of charge carriers and the mobility, related to traps present in the active layer, produced by the interaction of O_2 and H_2O.[30,32] On the other hand, the J_{SC} stability decay behaviour of OSCs can also be attributed to phase separation of the acceptor and donor domains, which diminishes the probability that charge carriers are collected in the electrodes and, as a result, a reduction of J_{SC} occurs.[47,48] This last one can be an explanation for the decay of J_{SC} in devices exposed to a N_2 atmosphere.

The FF of the NFA-OSCs for the three degradation conditions is shown in Fig. 2(d). For NFA-OSCs exposed to a N_2 atmosphere, the FF shows a similar trend to the PCE decay (see Fig. 2(a)). Therefore, we suggest that FF decay mainly dominates the degradation process in NFA-OSCs under a N_2 atmosphere. It is well known that lower mobility of the charge carriers leads to a longer carrier extraction time and, therefore, increases the probability of bimolecular recombination, which results in a reduced FF.[17,46] We observed that for non-encapsulated NFA-OSCs the FF reduces as the R_{Sh} decreases (Fig. 2(d) and (e)) for the entire analysis time, suggesting that this reduction of R_{Sh} is the main cause of the FF reduction due to a greater charge loss by recombination. After 336 h, similar behaviour is observed for encapsulated NFA-OSCs.

To obtain further analysis of the recombination within the devices, we carried out the fitting of the *J*–*V* characteristic under light using an equivalent circuit model consisting of three diodes (see Fig. S3†). The detailed fitting calculation can be found elsewhere.[17,49] Table S2† summarizes the parameters

Table 1 Parameters obtained from fitting the normalized PCE using eqn (1)

Conditions	A_1	T_1 [h]	A_2	T_2 [h]
N_2 atmosphere	0.20	7000	0.80	7000
Encapsulated	0.50	728	0.50	1400
Non-encapsulated	0.50	17	0.53	1372

extracted from the modelled *J–V* characteristic curves for fresh and degraded NFA-OSCs after 1000 h. All fresh NFA-OSCs show an ideal exponential region with an ideality factor n_1 in the range of 1.0 to 1.11. The ideality factor n_1 indicates the dominant transport mechanism in the active layer of the device. It is well known that if the predominant transport mechanism is diffusion then $n = 1$, and if the dominant transport mechanism is recombination, $n = 2$.[50] The values obtained for fresh NFA—OSCs indicate that the transport mechanism is mainly diffusion. Table S2† shows that the extracted ideality factors tend to increase over time as the devices degrade. It was observed that for NFA-OSCs under a N_2 atmosphere n_1 increased slightly, which suggests that the active layer was degrading slightly. For encapsulated and non-encapsulated NFA-OSCs, n_1 varies significantly from 1.11 to 1.40 and 1.50, respectively. These values after 1000 h can indicate a combination of monomolecular and bimolecular recombination processes.[51] In both devices, n_2 and n_3 become greater than 1, whereby the recombination mechanism seems to have some importance in the ETL/active layer/HTL interfaces of encapsulated and non-encapsulated NFA-OSCs. Table S2† further shows that the values of J_{01} increased over time for all the NFA-OSCs. In OSCs, J_{01} represents the minority charge density in the vicinity of the barrier present at the donor/acceptor interface in BHJ solar cells.[52] The greater the recombination in the active layer the greater the leakage current (J_{01}).[53] At the end of analysis time, if J_{01} has a higher value for non-encapsulated NFA-OSCs than for encapsulated NFA-OSCs, it can be implied that there is less recombination in encapsulated devices. The increase in J_{01} can be related to the presence of an additional source of minority charges near the heterojunction of the active layer.[54] Table S2† shows a larger reduction in the photogenerated current density (J_L) over time in encapsulated and non-encapsulated devices. For non-encapsulated devices, the photocurrent decreases by one magnitude order more than for encapsulated devices at the end of the analysis time. It is well known that the photocurrent represents the number of photogenerated charge carriers that become collected at the electrodes. The photocurrent is directly related to the EQE, which depends on the efficiencies of absorption, exciton dissociation, charge separation, and charge extraction.[55] In addition, when there is a low charge extraction rate it leads to space charge accumulation, and as a result, there is a major effect of recombination.[56] This behaviour is associated with s-shaped *J–V* characteristics.[26,57] Due to the aforementioned reasons, we can suggest that the charge extraction efficiency reduces more in non-encapsulated devices than in encapsulated devices. The *J–V* characteristics for non-encapsulated devices show an s-shape and as will be seen later these devices present major biomolecular recombination.

The external quantum efficiency (EQE) response over time was measured for encapsulated NFA-OSCs (see Fig. 3(a)), devices under a N_2 atmosphere (Fig. S4(a)†), and non-encapsulated devices (Fig. S4(b)†). All devices show a similar photoresponse for fresh cells from 300 nm to 1000 nm. The EQE response intensity in a short wavelength range of 300 nm to 400 nm is slightly low compared to the intensity at longer wavelengths, due to the limited absorption of the polymer donor (PM6) in this region.[3,58] It can be noticed in Fig. 3(a) and S4(b)† that the intensity of the spectrum decreased over time. This may indicate that the absorption efficiency and the separation, transport, and charge extraction in the encapsulated NFA-OSCs have degraded, which matches the decrease in J_{SC} observed in Fig. 2(c). As observed in detail in Fig. 3(a), it can be pointed out that the peak position at 820 nm decreased its intensity as compared to that of fresh devices for encapsulated NFA-OSCs. The peak locations in these range wavelengths (800–850 nm) are related to the absorption peaks of Y7, which are attributed to π–π staking, which provides more absorption from the Y7 acceptor that is efficiently converted into photocurrent.[59,60] Therefore, if in this wavelength region, the intensity of the EQE response is reduced, we can infer that the part of the photocurrent decreased due to the reductions of the π–π interactions. As a consequence, the J_{SC} is reduced over time. On the other hand, for devices exposed to a N_2 atmosphere, there was an inconsiderable diminution of the EQE response, indicating the most stable behaviour over time as compared to the

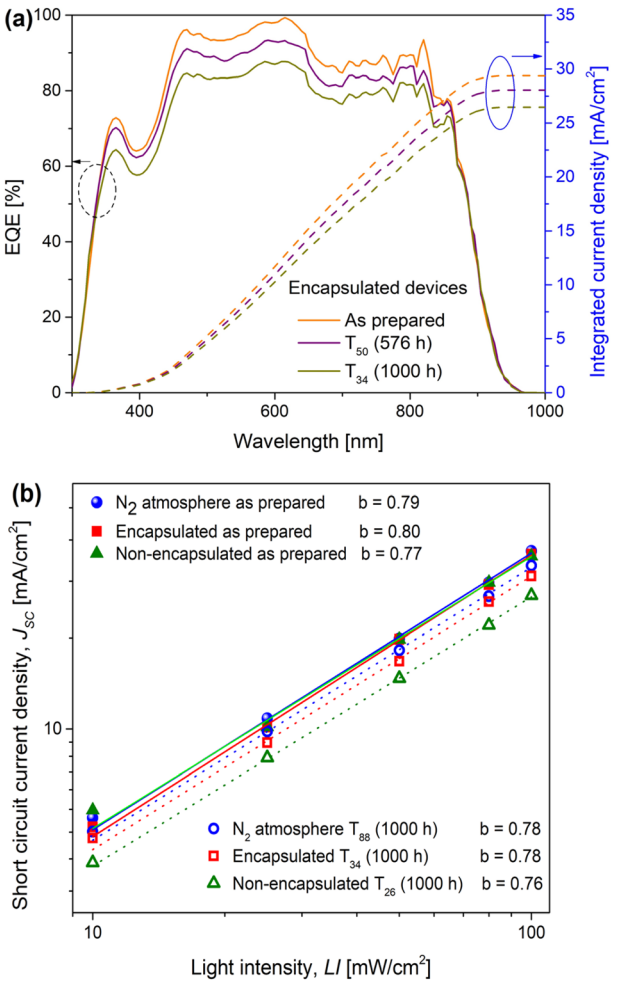

Fig. 3 (a) EQE spectra of the encapsulated NFA-OSCs; (b) J_{SC} as a function of light intensity of the NFA-OSCs under three conditions: N_2 atmosphere and encapsulated and non-encapsulated devices. Symbols show the experimental data and the solid and dotted lines show the fitted data using eqn (2).

fresh ones (Fig. S4†). This observed behaviour is coherent with the stabilized J_{SC} values obtained over time by the *J–V* characteristics in Fig. 2(c).

Additionally, in order to complement the information about the recombination mechanisms within the active layer of cells, we measured the dependence of J_{SC} on the incident light intensity (LI). The *J–V* characteristics of the NFA-OSCs were obtained at different LIs in the AM 1.5G spectrum. Fig. 3(b) shows the dependence of J_{SC} *vs.* LI on a log–log scale. A power-law dependence of J_{SC} under LI is generally observed in OSCs and can be expressed as:

$$J_{SC} \propto (LI)^b \quad (2)$$

where LI is the intensity of the light and *b* is the exponential factor. If *b* is close to 1, the bimolecular recombination is not significant.[7,51,61] The graph in Fig. 3(b) was fitted using a power law using eqn (2). The *b* values obtained varied from 0.79 to 0.78 for the NFA-OSCs exposed to the N_2 atmosphere. Similar values were obtained for encapsulated NFA-OSCs, from 0.80 to 0.78. Meanwhile, for non-encapsulated NFA-OSCs the obtained b values ranged from 0.77 to 0.76. The *b* values obtained for all the NFA-OSCs exposed to the three degradation conditions were less than 1 which indicates that the performances of devices decrease due to the effects of bimolecular recombination. In addition, we can see that the non-encapsulated NFA-OSCs suffer from a greater effect of bimolecular recombination than the other cells because the *b* values obtained were the lowest. This agrees with the obtained results by fitting *J–V* characteristics and from the aforementioned information about the FF, we can conclude that the reduction in the FF in encapsulated and non-encapsulated NFA-OSCS is due to the reduction of R_{Sh} as a result of the greater charge loss by recombination.

Impedance spectroscopy analysis

Impedance spectroscopy (IS) measurements were performed to analyse which layer of the NFA-OSCs is the most affected under the different degradation conditions. Fig. 4(a)–(c) show the experimental and fitted Cole–Cole plot of the IS data for N_2 atmosphere and encapsulated and non-encapsulated devices under AM 1.5G illumination for different degradation times. All the graphs show a semicircle form which is the classic behaviour of bulk heterojunction solar cells, attributed to the generation and recombination of charge carriers and charge transport.[4,62,63] It can be noticed that the Cole–Cole plot of the degraded NFA-OSCs has higher series resistance as well as a larger arc radius size than the fresh NFA-OSCs for all degradation conditions; the difference is more prominent at lower frequencies. In addition, the impedance arc at low frequency is an indication of charge accumulation that cannot be extracted by the contacts of the device.[64] Therefore, we can suggest that for the non-encapsulated NFA-OSCs, the charge extraction has been decreasing with respect to the encapsulated NFA-OSCs. This could confirm that the S-shape present in the last measure for non-encapsulated NFA-OSCs is caused by charge accumulation at the interfaces.[26,27]

To perform a deep study of the degraded NFA-OSCs, an equivalent electrical model is used to fit the experimental Cole–Cole plot[4,63,65,66] (see Fig. 4(f)). Every RC circuit is related to the

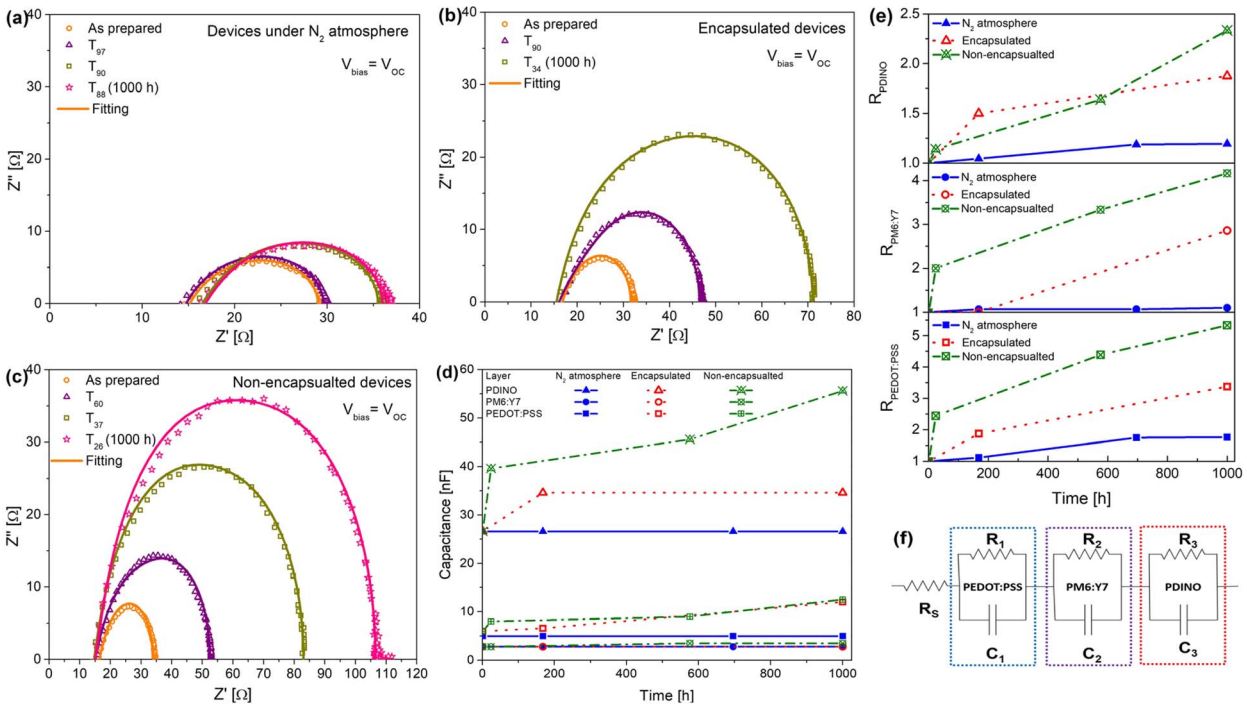

Fig. 4 Experimental impedance spectra at different times under AM 1.5 G illumination measured under open circuit conditions of NFA-OSCs exposed to three degradation conditions: (a) N_2 atmosphere, (b) encapsulated devices, and (c) non-encapsulated devices. Solid lines in (a)–(c) show the fitting results; (d) capacitance and (e) normalized resistance *vs.* time extracted from the fit using the RC circuital model shown in (f).

capacitance and resistance of each layer. In our case, we related capacitance C_1 to PEDOT:PSS, C_2 to PM6:Y7, and C_3 to PDINO. The three associated resistances (R_1, R_2, and R_3) to each capacitance were related to each layer, respectively. The series resistance (R_S) is needed to represent the ohmic contact resistance and wire effects, which are mostly related to substrate resistance. We found that the R_S value is low, from 3 Ω to 4 Ω, in all cells. Fig. 4(d) shows the capacitance values extracted from the equivalent electrical model. The geometric capacitance of each layer can be theoretically calculated as $C_g = \varepsilon\varepsilon_0 A/d$, where ε is the relative dielectric permittivity for the layer, ε_0 is the vacuum dielectric permittivity, A is the device area and d is the layer thickness. Table 2 shows the calculated capacitance values for each layer in the structure. These values were used to begin the fitting of IS measurements over time. From Fig. 4(d), we noticed three regions for capacitance values over time. The first region is above 26 nF, corresponding to PDINO. This capacitance shows the highest increase over time for non-encapsulated NFA-OSCs. The second region is between 5 nF and 10 nF corresponding to PEDOT:PSS. These values show slight and similar increases for both devices, encapsulated and non-encapsulated NFA-OSCs. The third region, around 3 nF, is related to the PM6:Y7 layer; for all degradation conditions these values have a minimum variation over time. This might indicate that at V_{OC}, the IS response was controlled by the geometrical capacitances of the active layer provided by the metal insulator-metal model indicating the presence of fully depleted layers.[67]

The normalized resistances (R) values as a function of the storage time are shown in Fig. 4(e). Table S3† shows the resistance values without normalization. The results show that the resistance for all layers in NFA-OSCs stored in a N_2 atmosphere varies slightly with degradation time. This is the reason why we can observe that PCE remained around 88% at the end of the analysis time. The layer that suffered from the least degradation was PM6:Y7 because it presented the least variation in R values. Concerning the encapsulated NFA-OSCs, the PDINO layer shows the least variation for R values. Notice that the R values for the active layer and PEDOT:PSS have the highest variation over time, whereby these layers govern the degradation behaviour of encapsulated NFA-OSCs. If these layers govern the performance over time, we can point out that the V_{OC} behaviour over time in encapsulated NFA-OSCs decreases due to charge recombination at the HTL/donor interface.[44] On the other hand, for non-encapsulated NFA-OSCs, the most important increase in the R values was observed for the PEDOT:PSS layer. Thus, the decrease in the performance of NFA-OSCs is mainly due to the degradation of the PEDOT:PSS. The PEDOT:PSS film exhibits poor stability when exposed to ambient conditions (oxygen and water). This confirms the "burn-in loss" effect observed in the performance parameters for the non-encapsulated NFA-OSCs, especially the V_{OC} and FF, which leads to their rapid degradation behaviour. In addition, compared with the encapsulated cells, the encapsulated stack provides enough protection to slightly reduce the degradation of the active layer and PEDOT:PSS. Therefore, to achieve long-term stable-OSCs it is necessary either to prepare a more stable PM6:Y7 blend *via* additive mediated aggregation control or/and to look for materials for replacing PEDOT:PSS. Zhang *et al.* showed that PCE for encapsulated inverted NFA-OSCs based on PM6:Y7 remained over 20% after 800 h.[68] On the other hand, Ahmad *et al.* showed that PCE for inverted NFA-OSCs based on PM6:Y7 stored in a N_2 atmosphere remained over 86% after 600 h.[69] Therefore, the selection of an adequate hole transport layer and blend engineering provides a promising strategy in NFA-OSCs since a longer lifetime can be obtained with a higher initial PCE value. Another promising strategy is the fabrication of layer-by-layer OSCs, which also exhibit better stability in comparison with bulk heterojunction OSCs.[70,71] Furthermore, a more efficient encapsulation process must be applied to achieve long-term stability.

Table 2 Dielectric constant, thickness, and calculated capacitance for each layer

Layers	ε_{layer}	d_{layer} [nm]	Capacitance [nF]
PEDOT:PSS	2.2	35	5
PM6:Y7	3.5[65]	100	2.79
PDINO	5[8]	15	26.5

Experimental section

Materials

The transparent conducting oxide used was an indium tin oxide (ITO) patterned glass substrate with a resistivity of 10 Ω sq^{-1} purchased from PsiOTec. PDINO, PM6 (poly[2,6-(4,8-bis(5-(2-ethylhexyl-3-fluoro)thiophen-2-yl)benzo [1,2-*b*;4,5*b*′]dithiophene))-*alt*-(5,5-(1′,3′-di-2-thienyl-5′,7′-bis(2-ethylhexyl)benzo [1′,2′-*c*:4′,5′-*c*′]dithiophene-4,8-dione)]) polymer donor and Y7 (2,2′-((2*Z*,2′*Z*)-((12,13-bis(2-ethylhexyl)-3,9-diundecyl-12,13-dihydro-[1,2,5]thiadiazolo[3,4-*e*]thieno[2″,3″:4′,5″]thieno[2′,3′:4,5] pyrrolo[3,2-*g*]thieno[2′,3′:4,5]thieno[3,2-*b*]indole-2,10-diyl)bis(-methanylylidene))bis(5,6-dichloro-3-oxo-2,3-dihydro-1*H*-indene-2,1-diylidene)) dimalononitrile) NFA were purchased from One-Material Inc. Chlorobenzene and 1-chloronaphthalene (CN) solvent and additive, respectively, were obtained from Sigma-Aldrich. A high-purity silver (Ag, 99.99%) wire was obtained from Testbourne Ltd.

Solar cell fabrication

The fabrication of the conventional NFA-OSCs was based on the structure of ITO/PEDOT:PSS/PM6:Y7/PDINO/Ag as shown in Fig. 1(a) which had been optimized in our previous work.[6] First, the ITO glass substrates were cleaned with deionized water/detergent and then sonicated in acetone, methanol, and isopropanol high-purity solvents in a sequence for 10 min, respectively. Then, the cleaned ITO glass substrates were dried in an oven at 100 °C for 10 min. Before fabrication, the substrates were treated with ultraviolet ozone for 15 min to eliminate any organic residues from their surface. The PEDOT:PSS solution was spin-coated on top of the precleaned ITO substrates at 4000 rpm for 40 s and then annealed in the air

for 15 min at 150 °C. The PEDOT:PSS-coated ITO substrates were placed into a nitrogen-filled glove box for active layer deposition. The PM6:Y7 blend with a weight ratio of 1 : 1 was dissolved in chlorobenzene (CB) and 1-chloronaphthalene (CN), (CB : CN = 99.5 : 0.5 by volume), to get 20 mg ml^{-1} of the total solution and left stirring for 3 h at 80 °C. Before the PM6:Y7 deposition step, the cooled down PEDOT:PSS film and the PM6:Y7 solution were both re-heated at 80 °C for 30 min. After 30 min, the hot solution of the PM6:Y7 blend was hot-deposited over the hot PEDOT:PSS film. Then, the PEDOT:PSS/PM6:Y7 films were left to anneal for 5 min at 90 °C. Afterward, the electron transport layer, PDINO (1.5 mg ml^{-1} in methanol) was deposited by spin coating at 3000 rpm for 30 s, obtaining a thickness of 15 nm. The substrates were finally transferred into an evaporation chamber inside the glove box where 100 nm Ag was deposited under high vacuum conditions (<1 × 10^{-6} mbar). The Ag film rate was 0.1 kÅ s^{-1} for the initial 10 nm thickness and then increased to 0.4 Å s^{-1} until 100 nm film thickness. The effective area of the devices was 0.09 cm^2.

Solar cell characterization

The current density–voltage (*J–V*) characteristics of the devices under light and dark conditions were obtained at room temperature with a Keithley 2400 source-measure unit using a solar simulator (Abet Technologies model 11000 class type A, Xenon arc). Calibration for the solar simulator intensity was performed with a Fraunhofer-certified photovoltaic cell to yield a 100 mW cm^{-2} and AM1.5G spectrum. J_{SC} over different light intensities was obtained by *J–V* measurements under the solar simulator using a set of optical density filters. The EQE spectra were recorded from 300 nm to 1100 nm using Lasing IPCE-DC model equipment with the series number LS1109-232. The impedance spectroscopy (IS) measurements were conducted under AM1.5G illumination conditions with an HP-4192A impedance analyser under open circuit conditions with 0.1 V amplitude in a frequency range of 5 Hz to 5 MHz. The devices were analysed for up to 1000 h under three different conditions: N_2 atmosphere and encapsulated and non-encapsulated devices.

Conclusions

We have investigated the lifetime and degradation of high-efficiency ITO/PEDOT:PSS/PM6:Y7/PDINO/Ag non-fullerene solar cells under three different degradation conditions: N_2 atmosphere and encapsulated and non-encapsulated devices by the analysis of the time evolution of current–voltage characteristics both under dark and illumination applying ISOS-D-1 protocols. The samples stored under a N_2 atmosphere and non-encapsulated and encapsulated devices have a lifetime (T_{80}) of ∼1000 h, ∼24 h, and 336 h, respectively. We showed that the evolution of the power conversion efficiency (PCE) can be fitted by the decaying of two exponentials with time constants T_1 and T_2. The values obtained from the fitting were associated with the predominant degradation mechanism, according to the degradation conditions. The degradation time constants obtained from the fitting for the devices under a N_2 atmosphere ($T_1 = T_2 = 7000$ h) reveal that only one degradation mechanism is involved. Due to the low quantity of oxygen and water in N_2 (<0.1 ppm), the mechanism responsible for the slow degradation was identified by the intrinsic chemical reactions between the metallic and organic materials. For the non-encapsulated devices, the degradation time constants were $T_1 = 17$ h and $T_2 = 1372$ h, which means that two degradation mechanisms are involved. The main degradation mechanism observed in this environment was due to water since it has the lowest degradation time constant. The mechanism responsible for the rapid degradation was related to the PEDOT:PSS layer due to its hygroscopic nature. Finally, for encapsulated devices, the degradation time constants were $T_1 = 728$ h and $T_2 = 1400$ h which means two degradation mechanisms were involved as well. The order of magnitude of the first time constant indicates that the degradation mechanism due to water is taking place more than that due to oxygen in encapsulated devices.

Based on the impedance spectroscopy results and the evolution of short circuit current density (J_{SC}) *versus* light intensity, we can suggest that poor stability of non-encapsulated devices is strongly associated with the oxidation of PEDOT:PSS by moisture, and these devices suffer from a significant loss of performance due to bimolecular recombination in comparison with those under other studied conditions. Finally, these results demonstrate that to obtain high-efficiency NFA-OSCs based on PM6:Y7 with a longer lifetime, a more efficient encapsulation process must be applied. Moreover, an adequate hole transport layer should be considered.

Conflicts of interest

The authors declare that there is no conflict of interest.

Acknowledgements

M. Ramírez-Como acknowledges the financial support from Diputació de Tarragona under Grant 2021CM14 and 2022PGR-DIPTA-URV04 and from Consejo Nacional de Ciencia y Tecnología (CONACYT) under program postdoctoral grants BP-PA-20220624083033039-2364083. This work was further supported by the Spanish Ministerio de Ciencia e Innovación (MICINN/FEDER) under Grants PDI2021-128342OB-I00, by the Agency for Management of University and Research Grants (AGAUR) ref. 2021-SGR-00739, and by the Catalan Institution for Research and Advanced Studies (ICREA) under the ICREA Academia Award.

References

1 J. Qin, Z. Chen, P. Bi, Y. Yang, J. Zhang, Z. Huang, Z. Wei, C. An, H. Yao, X. Hao, T. Zhang, Y. Cui, L. Hong, C. Liu, Y. Zu, C. He and J. Hou, *Energy Environ. Sci.*, 2021, **14**, 5903–5910.

2 J. Lv, H. Tang, J. Huang, C. Yan, K. Liu, Q. Yang, D. Hu, R. Singh, J. Lee, S. Lu, G. Li and Z. Kan, *Energy Environ. Sci.*, 2021, **14**, 3044–3052.

3 Q. Liu, Y. Jiang, K. Jin, J. Qin, J. Xu, W. Li, J. Xiong, J. Liu, Z. Xiao, K. Sun, S. Yang, X. Zhang and L. Ding, *Sci. Bull.*, 2020, **65**, 272–275.
4 M. Ramirez-Como, E. Moustafa, A. A. A. Torimtubun, J. G. Sanchez, J. Pallares and L. F. Marsal, in *2022 IEEE Latin American Electron Devices Conference (LAEDC)*, IEEE, 2022, pp. 1–5.
5 E. Moustafa, M. Méndez, J. Pallarès and L. F. Marsal, *Sol. Energy Mater. Sol. Cells*, 2022, **248**, 111985.
6 E. Moustafa, M. Méndez, J. G. Sánchez, J. Pallarès, E. Palomares and L. F. Marsal, *Adv. Energy Mater.*, 2023, **13**, 2203241.
7 J. Yuan, Y. Zhang, L. Zhou, G. Zhang, H. L. Yip, T. K. Lau, X. Lu, C. Zhu, H. Peng, P. A. Johnson, M. Leclerc, Y. Cao, J. Ulanski, Y. Li and Y. Zou, *Joule*, 2019, **3**, 1140–1151.
8 N. Tokmoldin, S. M. Hosseini, M. Raoufi, L. Q. Phuong, O. J. Sandberg, H. Guan, Y. Zou, D. Neher and S. Shoaee, *J. Mater. Chem. A*, 2020, **8**, 7854–7860.
9 Y. Cui, H. Yao, L. Hong, T. Zhang, Y. Tang, B. Lin, K. Xian, B. Gao, C. An, P. Bi, W. Ma and J. Hou, *Natl. Sci. Rev.*, 2020, **7**, 1239–1246.
10 D. Wang, H. Liu, Y. Li, G. Zhou, L. Zhan, H. Zhu, X. Lu, H. Chen and C.-Z. Li, *Joule*, 2021, **5**, 945–957.
11 L. Zhang, Z. Yao, H. Wang, J. Zhang, X. Ma and F. Zhang, *Solar RRL*, 2023, **7**(12), 2300219.
12 W. Xu, X. Ma, J. H. Son, S. Y. Jeong, L. Niu, C. Xu, S. Zhang, Z. Zhou, J. Gao, H. Y. Woo, J. Zhang, J. Wang and F. Zhang, *Small*, 2022, **18**(4), 2104215.
13 H. Zhou, L. Zhang, X. Ma, Y. Xibei, Y. Zheng, Z. Liu, X. Gao, J. Zhang, Z. Liu and F. Zhang, *Chem. Eng. J.*, 2023, **462**, 142327.
14 A. Sacramento, V. S. Balderrama, M. Ramirez-Como, J. G. Sanchez, M. Estrada and L. F. Marsal, in *2020 IEEE Latin America Electron Devices Conference (LAEDC)*, IEEE, San José, 2020, pp. 1–4.
15 M. Ramírez-Como, V. S. Balderrama, A. Sacramento, L. F. Marsal, G. Lastra and M. Estrada, *Sol. Energy*, 2019, **181**, 386–395.
16 L. Duan and A. Uddin, *Adv. Sci.*, 2020, **7**, 1903259.
17 M. Ramírez-Como, A. Sacramento, J. G. Sánchez, M. Estrada, J. Pallarès, V. S. Balderrama and L. F. Marsal, *Sol. Energy Mater. Sol. Cells*, 2021, **230**, 111265.
18 A. Sacramento, M. Ramirez-Como, V. S. Balderrama, S. I. Garduno, M. Estrada and L. F. Marsal, *IEEE J. Electron Devices Soc.*, 2020, **8**, 413–420.
19 S. K. Gupta, L. S. Pali and A. Garg, *Sol. Energy*, 2019, **178**, 133–141.
20 A. A. A. Torimtubun, J. G. Sánchez, J. Pallarès and L. F. Marsal, *Sustain. Energy Fuels*, 2020, **4**, 3378–3387.
21 E. Moustafa, J. G. Sánchez, L. F. Marsal and J. Pallarès, *ACS Appl. Energy Mater.*, 2021, **4**, 4099–4111.
22 J. G. Sánchez, V. S. Balderrama, M. Estrada, E. Osorio, J. Ferré-Borrull, L. F. Marsal and J. Pallarès, *Sol. Energy*, 2017, **150**, 147–155.
23 A. A. A. Torimtubun, J. Follana-Berná, J. G. Sánchez, J. Pallarès, Á. Sastre-Santos and L. F. Marsal, *ACS Appl. Energy Mater.*, 2021, **4**, 5201–5211.
24 A. A. A. Torimtubun, M. Méndez, J. G. Sánchez, J. Pallarès, E. Palomares and L. F. Marsal, *Sustain. Energy Fuels*, 2021, **5**, 6498–6508.
25 M. O. Reese, S. A. Gevorgyan, M. Jørgensen, E. Bundgaard, S. R. Kurtz, D. S. Ginley, D. C. Olson, M. T. Lloyd, P. Morvillo, E. A. Katz, A. Elschner, O. Haillant, T. R. Currier, V. Shrotriya, M. Hermenau, M. Riede, K. R. Kirov, G. Trimmel, T. Rath, O. Inganäs, F. Zhang, M. Andersson, K. Tvingstedt, M. Lira-Cantu, D. Laird, C. McGuiness, S. (Jimmy) Gowrisanker, M. Pannone, M. Xiao, J. Hauch, R. Steim, D. M. DeLongchamp, R. Rösch, H. Hoppe, N. Espinosa, A. Urbina, G. Yaman-Uzunoglu, J.-B. Bonekamp, A. J. J. M. van Breemen, C. Girotto, E. Voroshazi and F. C. Krebs, *Sol. Energy Mater. Sol. Cells*, 2011, **95**, 1253–1267.
26 A. Sundqvist, O. J. Sandberg, M. Nyman, J.-H. Smått and R. Österbacka, *Adv. Energy Mater.*, 2016, **6**, 1502265.
27 L. Zuo, J. Yao, H. Li and H. Chen, *Sol. Energy Mater. Sol. Cells*, 2014, **122**, 88–93.
28 C. H. Peters, I. T. Sachs-Quintana, W. R. Mateker, T. Heumueller, J. Rivnay, R. Noriega, Z. M. Beiley, E. T. Hoke, A. Salleo and M. D. McGehee, *Adv. Mater.*, 2012, **24**, 663–668.
29 A. V. Kesavan, K. K. Khanum, S. Subbiahraj and P. C. Ramamurthy, *J. Phys. Chem. C*, 2019, **123**, 22699–22705.
30 X. Wang, C. Xinxin Zhao, G. Xu, Z.-K. Chen and F. Zhu, *Sol. Energy Mater. Sol. Cells*, 2012, **104**, 1–6.
31 M. P. Nikiforov, J. Strzalka and S. B. Darling, *Sol. Energy Mater. Sol. Cells*, 2013, **110**, 36–42.
32 A. Sacramento, M. Ramírez-Como, V. S. Balderrama, J. G. Sánchez, J. Pallarès, L. F. Marsal and M. Estrada, *J. Mater. Chem. C*, 2021, **9**, 6518–6527.
33 H. bin Yang, Q. L. Song, C. Gong and C. M. Li, *Sol. Energy Mater. Sol. Cells*, 2010, **94**, 846–849.
34 F. Krebs, J. Carle, N. Cruysbagger, M. Andersen, M. Lilliedal, M. Hammond and S. Hvidt, *Sol. Energy Mater. Sol. Cells*, 2005, **86**, 499–516.
35 M. v. Madsen, *J. Photon. Energy*, 2011, **1**, 011104.
36 J. Cameron and P. J. Skabara, *Mater. Horiz.*, 2020, **7**, 1759–1772.
37 Y. Xia, G. Yan and J. Lin, *Nanomaterials*, 2021, **11**, 3119.
38 H. Alhummiany, S. Rafique and K. Sulaiman, *J. Phys. Chem. C*, 2017, **121**, 7649–7658.
39 Q. Lu, Z. Yang, X. Meng, Y. Yue, M. A. Ahmad, W. Zhang, S. Zhang, Y. Zhang, Z. Liu and W. Chen, *Adv. Funct. Mater.*, 2021, **31**, 2100151.
40 A. Kovrov, M. Helgesen, C. Boeffel, S. Kröpke and R. R. Søndergaard, *Sol. Energy Mater. Sol. Cells*, 2020, **204**, 110210.
41 Z. el Jouad, L. Cattin, M. Addou and J. C. Bernède, *Eur. Phys. J. Appl. Phys.*, 2019, **86**, 20201.
42 E. H. Chahid, M. Lotfi, O. Lotfi, M. A. Koumina, R. Heyd and A. Malaoui, *Int. J. Power Electron. Drive Syst.*, 2021, **12**, 1772.
43 K. Wang, Y. Zheng, G. Xu and X. Xu, *Prog. Nat. Sci.*, 2015, **25**, 323–326.
44 W. Tress, K. Leo and M. Riede, *Adv. Funct. Mater.*, 2011, **21**, 2140–2149.

45 N. Grossiord, J. M. Kroon, R. Andriessen and P. W. M. Blom, *Org. Electron.*, 2012, **13**, 432–456.
46 J. Schafferhans, A. Baumann, A. Wagenpfahl, C. Deibel and V. Dyakonov, *Org. Electron.*, 2010, **11**, 1693–1700.
47 D. Yang, F. C. Löhrer, V. Körstgens, A. Schreiber, S. Bernstorff, J. M. Buriak and P. Müller-Buschbaum, *ACS Energy Lett.*, 2019, **4**, 464–470.
48 V. S. Balderrama, F. Avila-Herrera, J. G. Sanchez, J. Pallares, O. Vigil-Galan, L. F. Marsal and M. Estrada, *IEEE J. Photovoltaics*, 2016, **6**, 491–497.
49 A. Sacramento, V. S. Balderrama, M. Ramírez-Como, L. F. Marsal and M. Estrada, *Sol. Energy*, 2020, **198**, 419–426.
50 T. Kirchartz, F. Deledalle, P. S. Tuladhar, J. R. Durrant and J. Nelson, *J. Phys. Chem. Lett.*, 2013, **4**, 2371–2376.
51 S. R. Cowan, A. Roy and A. J. Heeger, *Phys. Rev. B: Condens. Matter Mater. Phys.*, 2010, **82**, 245207.
52 C. Waldauf, M. C. Scharber, P. Schilinsky, J. A. Hauch and C. J. Brabec, *J. Appl. Phys.*, 2006, **99**, 104503.
53 V. S. Balderrama, F. Avila-Herrera, J. G. Sanchez, J. Pallares, O. Vigil-Galan, L. F. Marsal and M. Estrada, *IEEE J. Photovoltaics*, 2016, **6**, 491–497.
54 A. Kumar, R. Devine, C. Mayberry, B. Lei, G. Li and Y. Yang, *Adv. Funct. Mater.*, 2010, **20**, 2729–2736.
55 M. Stephen, K. Genevičius, G. Juška, K. Arlauskas and R. C. Hiorns, *Polym. Int.*, 2017, **66**, 13–25.
56 C. Deibel, A. Baumann and V. Dyakonov, in *Physics of Organic Semiconductors*, Wiley-VCH Verlag GmbH & Co. KGaA, Weinheim, Germany, 2013, pp. 575–602.
57 A. Wagenpfahl, D. Rauh, M. Binder, C. Deibel and V. Dyakonov, *Phys. Rev. B: Condens. Matter Mater. Phys.*, 2010, **82**(11), 115306.
58 Y. Cui, H. Yao, J. Zhang, T. Zhang, Y. Wang, L. Hong, K. Xian, B. Xu, S. Zhang, J. Peng, Z. Wei, F. Gao and J. Hou, *Nat. Commun.*, 2019, **10**, 1–8.
59 X. Wang, L. Zhang, L. Hu, Z. Xie, H. Mao, L. Tan, Y. Zhang and Y. Chen, *Adv. Funct. Mater.*, 2021, **31**, 2102291.
60 L. Zhan, S. Li, T.-K. Lau, Y. Cui, X. Lu, M. Shi, C.-Z. Li, H. Li, J. Hou and H. Chen, *Energy Environ. Sci.*, 2020, **13**, 635–645.
61 P. Hartnagel and T. Kirchartz, *Adv. Theory Simul.*, 2020, **3**, 2000116.
62 S. Engmann, H. W. Ro, A. A. Herzing, D. M. DeLongchamp, C. R. Snyder, L. J. Richter, A. Barito and D. J. Gundlach, *J. Mater. Chem. A*, 2017, **5**, 6893–6904.
63 E. von Hauff, *J. Phys. Chem. C*, 2019, **123**, 11329–11346.
64 B. Arredondo, M. B. Martín-López, B. Romero, R. Vergaz, P. Romero-Gomez and J. Martorell, *Sol. Energy Mater. Sol. Cells*, 2016, **144**, 422–428.
65 E. Moustafa, A. A. A. Torimtubun, J. Pallarès and L. F. Marsal, *Solar RRL*, 2021, 2100480.
66 R. C. I. MacKenzie, V. S. Balderrama, S. Schmeisser, R. Stoof, S. Greedy, J. Pallarès, L. F. Marsal, A. Chanaewa and E. von Hauff, *Adv. Energy Mater.*, 2016, **6**, 1501742.
67 H. Schroeder, *J. Appl. Phys.*, 2015, **117**, 215103.
68 X. Zhang, J. Cai, C. Guo, D. Li, B. Du, Y. Zhuang, S. Cheng, L. Wang, D. Liu and T. Wang, *Small*, 2021, **17**, 2102558.
69 N. Ahmad, L. Yanxun, X. Zhang, B. Wang, Y. Zhang and H. Zhou, *J. Mater. Chem. C*, 2020, **8**, 15795–15803.
70 X. Ma, W. Xu, Z. Liu, S. Y. Jeong, C. Xu, J. Zhang, H. Y. Woo, Z. Zhou and F. Zhang, *ACS Appl. Mater. Interfaces*, 2023, **15**, 7247–7254.
71 W. Xu, M. Zhang, X. Ma, X. Zhu, S. Y. Jeong, H. Y. Woo, J. Zhang, W. Du, J. Wang, X. Liu and F. Zhang, *Adv. Funct. Mater.*, 2023, 2215204.

